



Numerical study of a dimpled tube with conical turbulator using the first and second laws of thermodynamics

Shoab Khanmohammadi¹ · Ali Jahangiri² · Faezeh Nazari¹ · Neda Azimi^{3,4}

Received: 2 June 2022 / Accepted: 10 December 2022 / Published online: 18 January 2023
© Akadémiai Kiadó, Budapest, Hungary 2023

Abstract

The novelty of this numerical study is integrating strategy of dimpling the tube and using turbulators in the center of a tube under constant heat flux to improve heat transfer rate. This research focused on evaluating the effect of the geometric parameters in a dimpled tube equipped with a conical turbulator based on the first and second laws of thermodynamics. In CFD modeling, the uniform inlet velocity at the inlet of the dimpled tube, non-slip condition in the walls, and atmospheric pressure at the outlet of the dimpled tube, a uniform heat flux on the tube wall and an inlet temperature of 300 K are selected as boundary conditions. The effect of pitch (S) and number of dimples (N), Reynolds number (Re = in the range of 5000 to 20,000) and heat flux (3000, 5000, 10,000 W m⁻²) on entropy generation, Nusselt number and the pressure drop in a dimpled tube equipped with the turbulator was investigated. The results showed that increase in S reduces the Nusselt number, pressure drop and friction factor, but thermal entropy and friction entropy decrease and so the total entropy decreases. As the number of dimples increases, the Nusselt number increases, which has similar effect on the pressure drop and friction factor. Increase in the number of dimples leads to increase in the frictional and the overall entropy, but decrease in the thermal entropy. The results showed that in low Reynolds number, the share of thermal entropy generation is much higher than the friction entropy generation and as the Reynolds number increases the share of friction entropy generation in the total entropy generation increases. The maximum Nusselt number and friction factor are related to $Re = 20,000$, $S = 14$ mm and $N = 4$. Based on the obtained data from modeling, heat flux has not significant influence on heat transfer and pressure drop. The maximum thermal entropy and total entropy are at $Re = 5000$, $S = 14$ mm and $N = 2$, while the highest friction entropy is related to $Re = 5000$, $S = 14$ mm, $N = 4$ and heat flux = 10,000 W m⁻². Finally, the results of this research confirm that the dimples on the tube body and inserting the turbulator in the center of the dimpled tube with the efficient pitch and the number of dimples can be a logical technique to intensify the heat transfer process.

Keywords Heat transfer · Turbulator · Dimple · Pitch · Heat exchanger · First law · Second law

Introduction

Today, with the advancement of technology, one of the most important engineering challenges is to increase heat transfer and improve the performance of heating systems. By growing and development of modern technologies, special attention has been paid to heat transfer, reducing heat transfer time, minimizing the size of heat exchangers and finally maximizing the efficiency of heating equipment [1]. As mentioned, due to energy constraints and the fact that the world is moving toward energy storage and using net-zero energy systems, it is necessary to optimize heating systems and increase heat transfer, one of which is heat exchangers [2–4]. One of the techniques to increase the heat transfer rate is to increase the level of heat exchange by using

✉ Shoab Khanmohammadi
sh.khanmohammadi@kut.ac.ir

¹ Department of Mechanical Engineering, Kermanshah University of Technology, Kermanshah, Iran

² Faculty of Mechanical and Energy Engineering, Shahid Beheshti University, Tehran, Iran

³ Chemical Engineering Department, CFD Research Center, Razi University, Kermanshah, Iran

⁴ Department of Chemical Engineering, Kermanshah Branch, Islamic Azad University, Kermanshah, Iran

tubes with protrusions and dimples [5]. Dimple tubes are in fact smooth tubes that have indentation on their walls that increase the level of heat transfer and thus increase heat transfer [6]. Dimples act as vortices to create turbulent flow in the flow to increase heat transfer. Recent researches show that dimpled surfaces can increase the rate of convective heat transfer and decrease the relative pressure [5], [7]. Due to the suitability of submerged surfaces in improving heat transfer, many experimental and numerical studies have been performed in recent decades [8].

Wang et al. [9] investigated the performance of protruding and dimpled tubes using air-operated fluid and proposed relationships to predict heat transfer and pressure drop. Kumar et al. [10] performed experiments on dimpled tubes. They found that most tube hydraulics have a indentation of 14–56% more than flat tubes. Li et al. [11] experimentally examined dimpled tubes in in-tube heat exchangers. They found that the increase in heat transfer compared to a flat tube was 200%. Kukulka et al. [12] performed experiments on the condensation and evaporation of dimpled tubes, which they called Vipertex tubes. They reported that Vipertex tubes evaporate well because indentations increase surface turbulence and boundary layer distribution. Shafae et al. [13] investigated the thermal performance of dimpled tubes for both deep and shallow indentations using R-600 operating fluid. Experiments have shown that tubes with dents (dimples) increase the heat transfer coefficient by 29–100% compared to simple tubes. Aroonrat and Wongwises [14], [15] experimentally studied biphasic density on hydraulic heat performance in dimpled tubes. They found that dimpled tubes resulted in the highest Nusselt number being about 84% higher than flat tubes. Chen et al. [16] performed experiments on tubes with two three-dimensional diagonal grooves and proposed relationships to predict the heat transfer coefficient. Cheng et al. [17] measured the Nusselt numerical distribution and the pressure drop coefficient for four hexagonal channels with dimpled walls and obtained relationships for each of the tubes. Xie et al. [18] developed a complex geometry using the plastic forming method for tube reinforced with indentations and ridges and discussed its heat-hydraulic performance. They found that the protrusions cause the flow of the fluid to rot and block the flow in the ridges and indentations, thus increasing the rate of heat transfer.

Another way to increase heat transfer is to use turbulator which are one of the tools that increase heat transfer by disturbing the flow of fluid. Turbulators are usually spiral blades that are inserted into boiler tubes, heat exchangers, boiler chimneys, aircraft fins, and fiberglass boilers to rotate the flow [19]. Turbulators are fixed or vibrant mechanical components that increase the heat transfer coefficient by creating turbulence in the flow and destroying the boundary layer, preventing sediment on the inner surface of the

tube and prolonging the flow path in the tube, resulting in more fluid flow time [20]. Contact is achieved by the heat exchange surface and the heat transfer rate increases. Some studies focused on the properties of the operating fluid and improving it, and some others focused on active and inactive methods for heat exchanger optimization. Changes in geometric parameters and other effective factors to improve heat transfer have been extensively investigated by scholars. When a fluid passes through a tube, the part of the fluid that is close to the tube wall is cooled due to friction with the wall and the low passage rate, and the rest of the fluid have less heat transfer, as a result, heat transfer around the tube will be less. In addition, the fluid flow in the tube and heat exchangers tends toward the wall of the tube, which acts both as an insulating layer and causes sediment in the walls. The turbulator breaks this layer by creating turbulence in the flow and converts the flow regime from laminar to turbulent regime, thus increasing heat transfer and less sediment. Eiamsa-ard and Promvonge [22] performed an experimental study of the effect of a helical strip inside a circular tube on the Nusselt number at Reynolds 2300 to 8800. They showed that the highest heat transfer rate occurs by placing the full length of the helical strip with the central rod in a flat tube. Jasinski [23, 24] performed two numerical studies on the thermo-hydraulic properties of a circular tube equipped with a ball-shaped turbulator. These researches consisted of two phases (the second phase focuses on the heat transfer process), the first of which presents the numerical simulation results in a circular tube with an internal ball flowing. The obtained results show a good correlation between computer testing and modeling. Several studies that focused on using turbulators to improve the heat transfer rate in heat exchangers are illustrated in Table 1.

After comprehensively considering aforementioned studies, we can see that there is rare studies focused on using turbulators in dimpled tubes based on the first and second law of thermodynamics. Adding dimples on the inner bodies of the tubes can be favorable to increase the heat transfer coefficient with a consequent rise in the friction factor and interruption of the boundary layer, increase the turbulence and effective heat transfer area and generation of secondary flows [34], [35]. Generally, by reviewing similar studies published in the mentioned researches reviewed above, it can be said that there is no complete and comprehensive study that investigates heat transfer in dimple tubes equipped with turbulators. The effect of pitch (S) and the number of dimples (N) in three heat fluxes applied to the dimple tube has been investigated. The important point in this research is the numerical investigation of the Nusselt number and the first and second laws of thermodynamics to obtain the effect of the Reynolds number and the mentioned parameters on the heat transfer

Table 1 Summarized list of some studies that used turbulators in heat exchangers

Refs.	Type of turbulator	Heat exchanging system	Output
[25]	Dolphin's dorsal fin turbulators (DFTs)	A counter flow double-pipe heat exchanger	DFTs improves heat transfer rate by colliding the fluid stream and destruction the boundary layer
[26]	Novel turbulators	Rectangular channel	The enhancement in the thermo-hydraulic performance evaluation criterion (THPEC) of the heat exchanger with the innovative and conventional turbulators is 13 and 23%, respectively, more than that of without turbulator
[27]	A dual twisted tape turbulator	A double-tube heat exchanger	1-Heat transfer in the heat exchanger equipped with twisted tape turbulator is up to 2.02 times the simple heat exchanger 2-Nusslte number rises with reduction in turbulator ratio
[28]	Helical baffle turbulators	A concentric double-tube heat exchanger	Increase in the heat transfer (η_{TPF}) by using turbulators with different pitch distances of 260, 108.57, 67.27 and 48 mm is 2.36, 2.42, 2.53 and 2.71, respectively
[29]	Zigzag shaped turbulators	A concentric pipe heat exchanger	The augmentation of the heat transfers in the heat exchanger equipped with different type of turbulators comparatively to the simple pipe is 5–75%
[30]	Semicircular striped turbulators	Coaxial heat exchanger	Nusselt number and friction factor values increased by 5.43 and 4.71 times, respectively, compared to the simple pipe, and the TPF raised up to the value of 3.72
[31]	Perforated turbulators	A double-pipe heat exchanger	Heat transfer in heat exchanger equipped with innovative perforated turbulators is increased up to 133.2% compared to the simple one
[32]	Wavy turbulators	Compact heat exchangers	Using turbulators led to improve the performance of the heat exchanger for the tested conditions
[33]	Wing-shaped turbulators	A serpentine heat exchanger	Installing the wing-shaped turbulators on the outer wall and inner wall of heat exchanger supplied the strong helical flow along the two straight passages. Therefore, the positive effect of turbulators on heat transfer was seen
[21]	Helical wire turbulator	A shell-coiled tube heat exchanger	It was observed that applying turbulators for helical tubes could improve the heat transfer rate

rate and entropy generation. The novelty of this research is the integration of both turbulence factors in the tube, i.e., dimpling on the tube and also placing the turbulator in the centerline of tube. Dimpling the tube leads to disrupting the boundary layer, creating turbulence, as well as increasing the effective surface area, friction coefficient, and ultimately improving heat transfer. On the other hand, the presence of the turbulator leads to the prolonging the flow path in the tube in addition to the effects mentioned for the dimples. Many studies in the field of only dimpling the tube and only placing the turbulator in the tubes can be found in the literature. However, the integration of these two passive methods to intensify the heat transfer in the tubes under the heat flux has not been done numerically so far. Investigating this issue from the point of view of the first and second laws of thermodynamics is a significant issue. On the other hand, this idea can be considered as a net-zero issue because it is passive and does not use any

external energy to improve heat transfer. Briefly, it can be said that the objectives of this research are as follows:

- This research focused on optimizing the geometric parameters in a dimpled tube equipped with a conical turbulator based on the first and second laws of thermodynamics.
- The investigated dimpled tube is equipped the cones, which are installed on a narrow rod in the center of the tube.
- The first main aim is to investigate the effect of geometric parameters such as pitch (S) and number of dimples (N), Reynolds number (Re = in the range of 5000 to 20,000) and heat flux (3000, 5000, 10,000 ($W m^{-2}$)) on entropy generation, Nusselt number and the pressure drop in the dimpled tube with turbulator.
- The second aim is to investigate the effect of turbulator geometric parameters on entropy generation and to find

the relationship between them and also to evaluate heat transfer and pressure drop to achieve more optimal conditions.

Numerical modeling

Physical model and geometry

Cone turbulence means that the cones are mounted on a narrow bar in the center of the dimpled tube. For this purpose, a tube with a length of 100 mm and diameter of 20 mm with a turbulator with a diameter of 1 mm in the center is investigated, and its schematic is shown in Fig. 1.

The governing equations

The numerical simulation involves solving basic conservation equations. The governing equations in this research are as follows[33]–[38]:

Continuity equation:

$$\frac{\partial}{\partial x_i}(\rho u_i) = 0 \quad (1)$$

Momentum equation:

$$\frac{\partial}{\partial x_j}(u_j \rho u_i) = -\frac{\partial p}{\partial x_i} + \frac{\partial}{\partial x_j}[-\rho \overline{u'_i u'_j}] + \frac{\partial}{\partial x_i} \left\{ \mu \left[\frac{\partial u_i}{\partial x_j} + \frac{\partial u_j}{\partial x_i} \right] \right\} \quad (2)$$

Energy equation:

$$\frac{\partial}{\partial x_j}(\rho u_j T) = \frac{\partial}{\partial x_i} \left\{ \left[\frac{\mu}{Pr} + \frac{\mu_t}{Pr_t} \right] \frac{\partial T}{\partial x_i} \right\} \quad (3)$$

Reynolds stress:

$$-\overline{\rho u'_i u'_j} = \mu_t \left[\frac{\partial u_i}{\partial x_j} + \frac{\partial u_j}{\partial x_i} \right] - \frac{2}{3} \rho k \delta_{ij} - \frac{2}{3} \mu_t \frac{\partial u_k}{\partial x_k} \delta_{ij} \quad (4)$$

Confused viscosity:

$$\mu_t = \rho C_\mu \frac{K^2}{\varepsilon} \quad (5)$$

Equations of k and ε for turbulent flow model:

$$\frac{\partial}{\partial x_i}(\rho u_i k) = \frac{\partial}{\partial x_j} \left\{ \left[\frac{\mu_t}{\sigma_k} + \mu \right] \frac{\partial k}{\partial x_j} \right\} + G_k - \rho \varepsilon \quad (6)$$

$$\frac{\partial}{\partial x_i}(\rho u_i \varepsilon) = \frac{\partial}{\partial x_j} \left\{ \left[\frac{\mu_t}{\sigma_\varepsilon} + \mu \right] \frac{\partial \varepsilon}{\partial x_j} \right\} + \frac{\varepsilon}{k} [C_{1\varepsilon} G_k - \rho C_{2\varepsilon} \varepsilon]$$

$$G_k = -\overline{\rho u'_i u'_j} \frac{\partial u_j}{\partial x_i} \quad (7)$$

The constant coefficients selected in the k - ε equation (RNG model) are as follows:

$$C_{1\varepsilon} = 1.42, C_{2\varepsilon} = 1.68, C_\mu = 0.0845, Pr_t = 0.85, \sigma_k = 1, \sigma_\varepsilon = 1.3$$

Boundary conditions

The boundary conditions include uniform inlet velocity at the inlet of the dimpled tube, non-slip condition in the walls, and atmospheric pressure at the outlet of the dimpled tube. Temperature boundary conditions also include the application of a uniform heat flux on the tube wall and an inlet temperature of 300 K. The mathematical form of boundary conditions is as follows:

Inputs:

$$u = u_0; T = T_0 \quad (8)$$

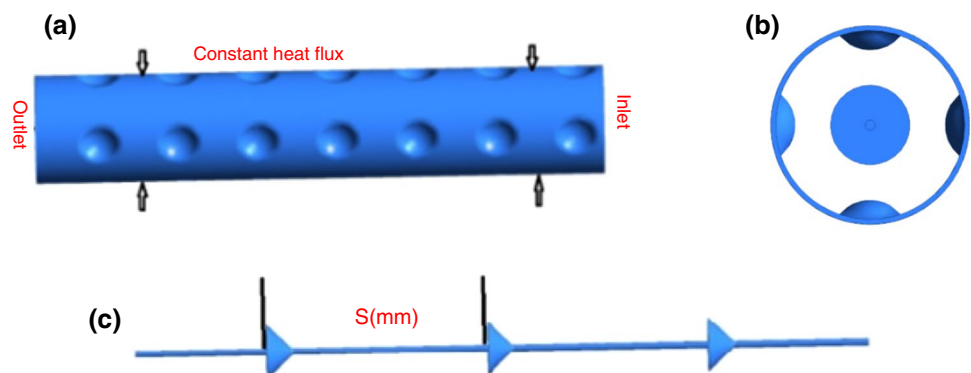
Boundary between solid and liquid:

$$u = 0; -k \frac{\partial T}{\partial y} = q'' \quad (9)$$

Outputs:

$$p = p_0 \quad (10)$$

Fig. 1 **a** Schematic of the dimpled tube and a constant heat flux applied to its sidewall, **b** facing view of turbulator and tube, **c** side view of the turbulator



Heat transfer performance and entropy generation

Using Eq. (11), the Reynolds number (Re) can be calculated, which is an indicator of the type of flow (laminar or turbulent):

$$Re = \frac{\rho u D}{\mu} \tag{11}$$

where μ is the dynamic viscosity, ρ is the density, u is the flow velocity, and D is the diameter of the tube [39], [40].

Equation (12) is used to calculate the Nusselt number (Nu). Here, h is the convective heat transfer coefficient and k is the conduction heat transfer coefficient [36]–[41]:

$$Nu = \frac{hD}{k} \tag{12}$$

Using Eq. (13), the friction coefficient (f) can be calculated as follows [36]–[41]:

$$f = \frac{2D}{L} \frac{\Delta p}{\rho u^2} \tag{13}$$

where Δp is the pressure drop, u velocity and L is the length of the tube.

Overall entropy [42]:

$$S_t = S_f + S_{th} \tag{14}$$

Thermal entropy [43]:

$$S_{th} = \frac{k}{T^2} \left[\left(\frac{\partial T}{\partial x} \right)^2 + \left(\frac{\partial T}{\partial y} \right)^2 + \left(\frac{\partial T}{\partial z} \right)^2 \right] \tag{15}$$

Frictional entropy [43]:

$$S_f = \frac{\mu}{T} \left\{ 2 \left[\left(\frac{\partial u_x}{\partial x} \right)^2 + \left(\frac{\partial u_y}{\partial y} \right)^2 + \left(\frac{\partial u_z}{\partial z} \right)^2 \right] + \left(\frac{\partial u_x}{\partial y} + \frac{\partial u_y}{\partial x} \right)^2 + \left(\frac{\partial u_x}{\partial z} + \frac{\partial u_z}{\partial x} \right)^2 + \left(\frac{\partial u_y}{\partial z} + \frac{\partial u_z}{\partial y} \right)^2 \right\} \tag{16}$$

Grid independence and model validation

In order to find the correct grid number to solve the equations numerically, it is necessary to examine the dependence of the results on the number of grids. For this purpose, the number of computational domain grids gradually is increased, and the results in each case are recorded. In the end, when the results do not change, the number of grids is acceptable, and there is no need to make the grid smaller and increase the computational cost. In Table 2, grid independence is evaluated in two $Re = 10,000$ and $15,000$. According to the diagram shown in Fig. 2, there is no change in the Nusselt number by increasing the number of cells. In addition, according to the diagram in Fig. 3, the friction coefficient does not change or these changes are so small that they are ignored, so that to save time and reduce the computational cost, approximately 804,963 cells are enough for the computing grid, and reliable answers can be obtained. Therefore, this number of grids is considered in this study.

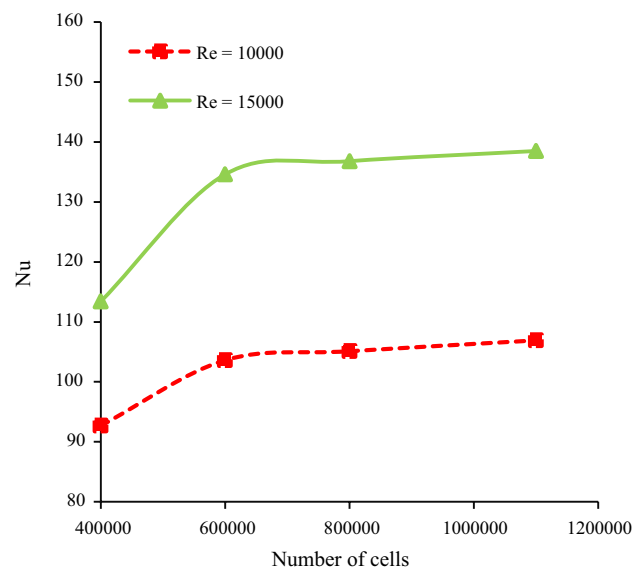


Fig. 2 Changes in Nu versus the number of cells for two different Reynolds numbers

Table 2 Investigation of Nusselt number changes and friction factor

Number of cells/–		Nu/–		Number of cells/–		f/–		Different f/%	
Re	Re	Re	Re	Re	Re	Re	Re	Re	Re
10,000	15,000	10,000	15,000	10,000	15,000	10,000	15,000	10,000	15,000
410,029	410,029	92.08103	113.3787	9.116	14.62	0.397292	0.367275	12.281	15.3421
610,274	610,274	101.3171	132.8021	1.571	1.996	0.452916	0.43384	1.64	2.16
804,963	804,963	102.9347	135.5069	1.182	1.1	0.460472	0.443452	0.923	1.5
1,108,520	1,108,520	104.1667	137.146	–	–	0.464766	0.450285	–	–

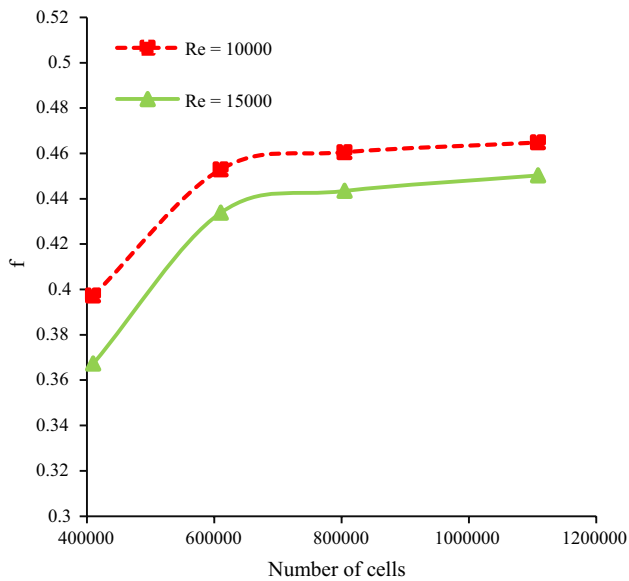


Fig. 3 Changes in the friction factor versus the number of cells for two different Reynolds numbers

The following table is for pitch (S) = 14 mm and the number of dimples (N) = 2.

After modeling the system geometry and checking the independence of the grid, the results should be compared and evaluated with the results that have already been obtained numerically or experimentally. Therefore, the results were compared with the results presented by Xie et al. [18], which is a study on the characteristics of flow and heat transfer in dimple tubes with tear dimples. The Reynolds number changed between 5000 and 30,000.

According to Fig. 4, the numerical results obtained for the Nusselt number are well-consistent with the results presented by Xie et al. [18], in which case the deviation rate of these results is 5.54%.

Results and discussion

Effect of pitch

Effect of pitch on pressure drop, velocity distribution and Nusselt number

Figure 5 shows the pressure drop changes versus pitch (S) in different Reynolds numbers for the flux of $10,000 \text{ W m}^{-2}$ at the number of dimples of 3 ($N=3$). As can be seen, the pressure drop decreases with increasing pitch (S). In fact, with increasing pitch, the number of cones decreases and the pressure drop decreases.

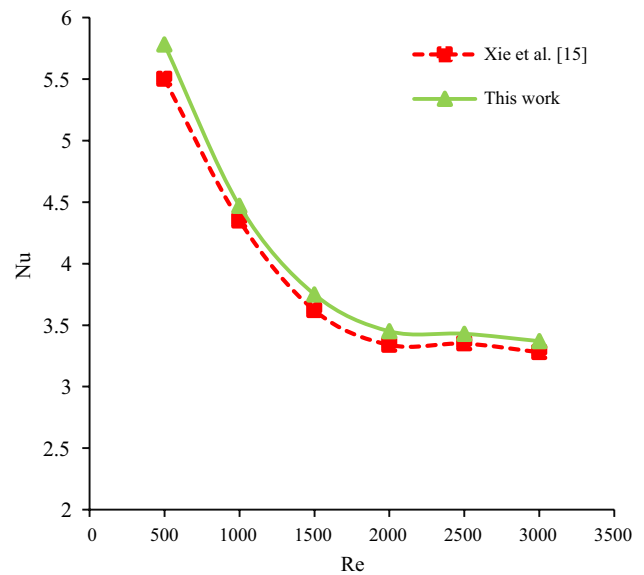


Fig. 4 Comparison of Nusselt number versus Reynolds number in Xie et al. [18] with numerical results obtained in this study

Figure 6 shows the pressure contours for pitches, $S = 14$, 22 and 30 mm at $Re = 20,000$. According to this figure, in the pitch of $S = 14$ mm, the maximum pressure drop is observed, which occurs due to the friction between the fluid with the wall and the cones. As the pitch decreases, the number of conical turbulator increases due to the turbulence of the flow and fluid friction. Therefore, increasing the pitch reduces the friction coefficient and pressure drop.

Figure 7 shows the velocity contours for different pitches at $N = 3$ in $Re = 10,000$. Figure 8 shows the changes of the

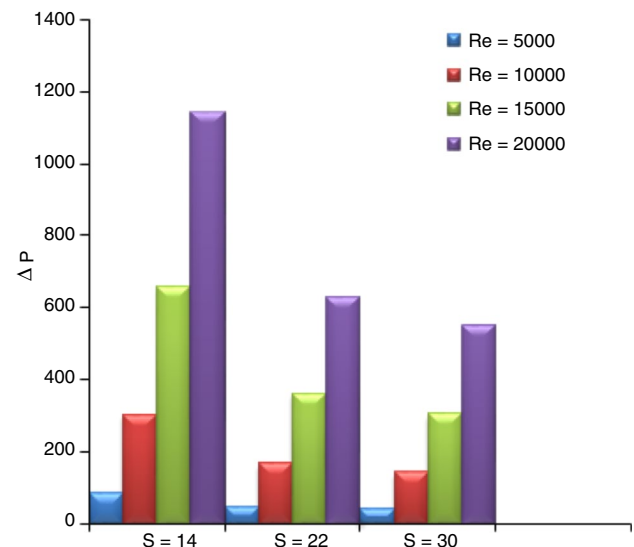


Fig. 5 Pressure drop changes versus pitch (S) in different Reynolds numbers for flux (W m^{-2}) of 10,000 and $N = 3$

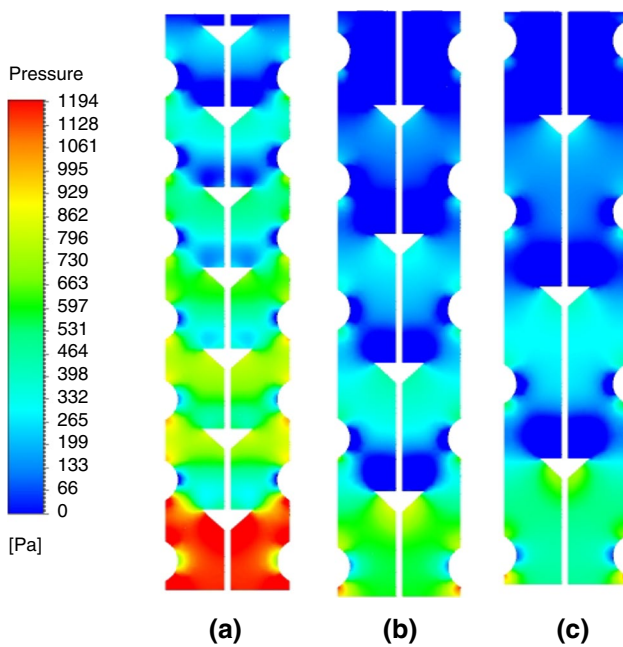


Fig. 6 Pressure contour for different pitches in $Re=20,000$: a $S=14$ mm, b $S=22$ mm, c $S=30$ mm

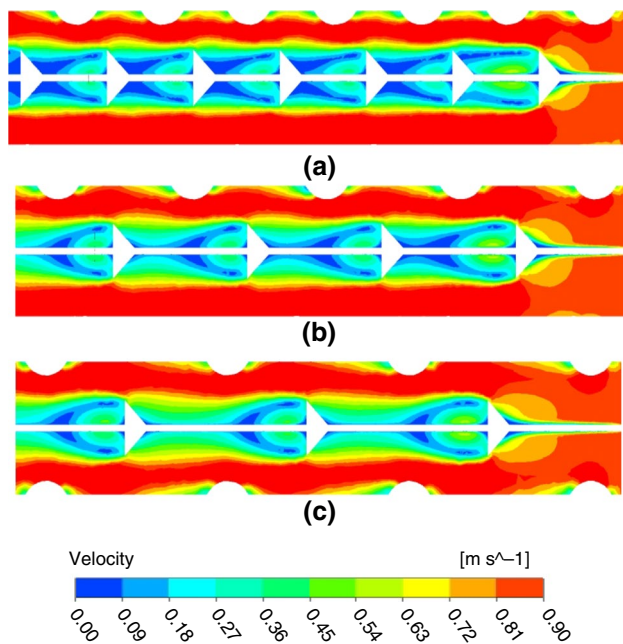


Fig. 7 Velocity contours for different pitches in $Re=10,000$: a $S=14$ mm, b $S=22$ mm, c $S=30$ mm

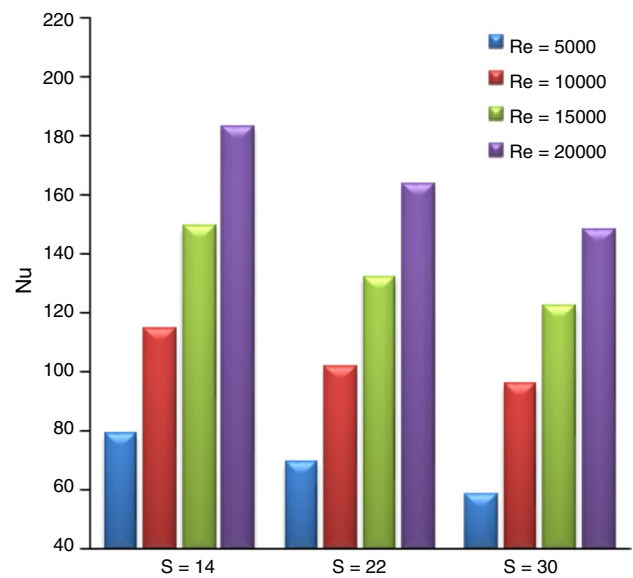


Fig. 8 Variation in Nusselt number versus pitch (S) in different Reynolds numbers for $q=10,000$ ($W\ m^{-2}$) and $N=4$

Nusselt number versus pitch in different Reynolds numbers at the heat flux ($W\ m^{-2}$) of 10,000. It is clear that as the pitch increases, the Nusselt number decreases. In fact, as the pitch increases, the number of cones decreases and the flow turbulence decreases. In addition, reducing the temperature gradient near the wall reduces the heat transfer coefficient and reduces the heat transfer. As the pitch decreases, in fact, the number of cones increases, and consequently, the turbulence of the flow and the turbulence of the thermal boundary layer increase. The rate of heat exchange also increases, which increases the displacement heat transfer coefficient, which is directly related to the Nusselt number. Therefore, decreasing the pitch increases the Nusselt number and increases the heat transfer.

Effect of pitch on entropy generation

As mentioned in the previous sections, variations in the friction entropy are a function of changes in velocity gradient. Here, the process of changing the friction entropy based on the pitch is investigated. Figure 9 shows the frictional and thermal entropy changes in Reynolds numbers at different pitches for $N=2$ and $q''=3000\ W\ m^{-2}$. The pitch is actually the distance between the two cones inserted on the center

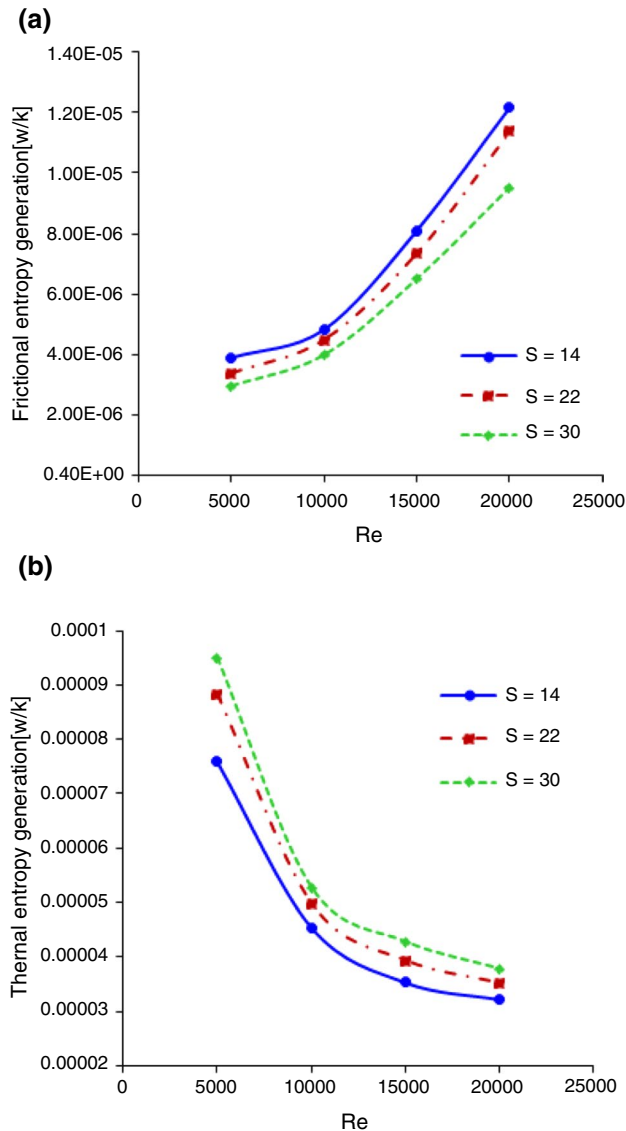


Fig. 9 Changes in **a** Frictional entropy generation, and **b** thermal entropy generation changes versus Re in different pitches for $q'' = 3000 \text{ W m}^{-2}$ and $N = 2$

bar, and as the number of pitches increases, the number of cones decreases. Therefore, it can be concluded that increasing the pitch or decreasing the number of cones reduces the velocity gradient. As the number of cones decreases, the number of obstacles in front of the flow decreases and the velocity gradient, which represents velocity changes, decreases, causing the frictional entropy to decrease. Therefore, as shown in Fig. 9a, at a constant Reynolds number, as the pitch increases, the friction entropy decreases so that the minimum friction entropy is related to the pitch of $S = 30 \text{ mm}$.

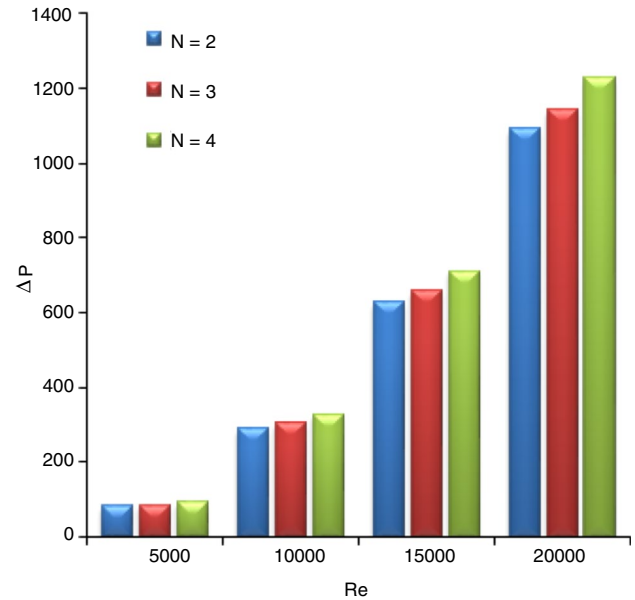


Fig. 10 Variation of the pressure drop versus Reynolds number for different N for $S = 14 \text{ mm}$ and $q = 5000 \text{ W m}^{-2}$

Figure 9b shows a graph of thermal entropy changes under the mentioned conditions in Fig. 9a. At a constant Reynolds number, the higher the pitch results in the higher the thermal entropy. According to Eq. (15), thermal entropy is directly related to temperature gradient. The greater pitch leads to the higher the temperature gradient in the wall and the higher the thermal entropy. Figure 9b shows that the maximum thermal entropy is related to the pitch of $S = 30 \text{ mm}$ and the $Re = 5000$.

Investigating the effect of Reynolds number

Figure 10 shows the pressure drop changes versus Reynolds number at different N for $S = 14 \text{ mm}$ at $q'' = 5000 \text{ W m}^{-2}$. The pressure drop increases with increasing Reynolds number. In fact, the higher the Reynolds number causes increasing the flow friction with the tube wall and turbulator. Figure 11 shows the velocity contours in different Reynolds numbers for $S = 22 \text{ mm}$ and $N = 4$.

Figure 12 shows the variation of the Nusselt number versus Reynolds number in the different number of dimples for $q'' = 5000 \text{ W m}^{-2}$. As can be seen, with increasing Reynolds number, Nusselt number rises because this boosts the turbulence of the flow and thus the heat transfer rate. The reason can be explained by the fact that since the inlet temperature and heat flux have constant values, so with reducing the outlet temperature, the temperature difference decreases and based on the relationship of heat transfer coefficient of convection ($h = q''/\Delta T$), which can be said to increase h.

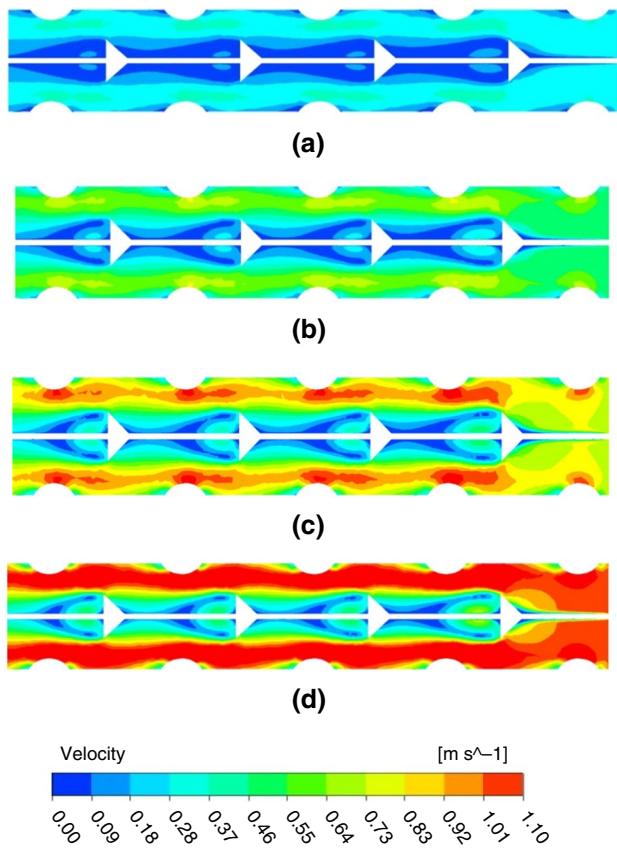


Fig. 11 Velocity contour in different Reynolds numbers for $S=22$ mm and $N=4$ for **a** $Re=5000$, **b** $Re=10,000$, **c** $Re=15,000$, **d** $Re=20,000$

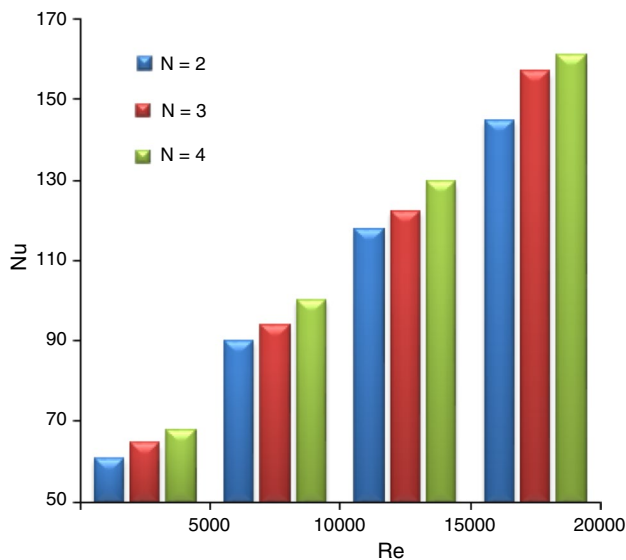


Fig. 12 Variations of the Nusselt number versus Reynolds number in different N for $q''=5000$ $W\ m^{-2}$ and $S=30$ mm

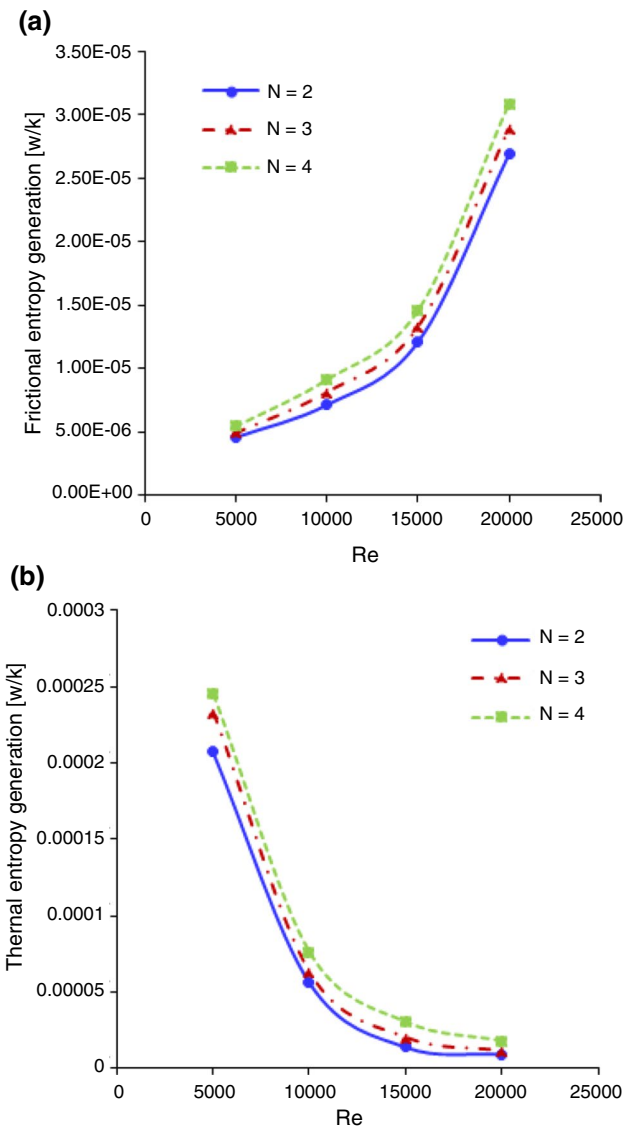


Fig. 13 Changes of **a** frictional entropy, **b** thermal entropy versus Reynolds number in different N for $q''=10,000$ $W\ m^{-2}$ and $S=30$ mm

The total entropy is equal to the sum of the frictional and thermal entropies. First, the effect of Reynolds number on the generation of friction entropy is investigated. According to Eq. (16), changes in velocity gradient determine the amount and trend of friction entropy generation. As the Reynolds number increases, the gradient increases, and the frictional entropy also increases. Figure 13a shows the changes in friction entropy versus Reynolds number at $S=30$ mm and different N . It is clear that as the Reynolds number increases, the frictional entropy also increases.

The second part of total entropy generating is thermal entropy, which is a function of temperature gradient.

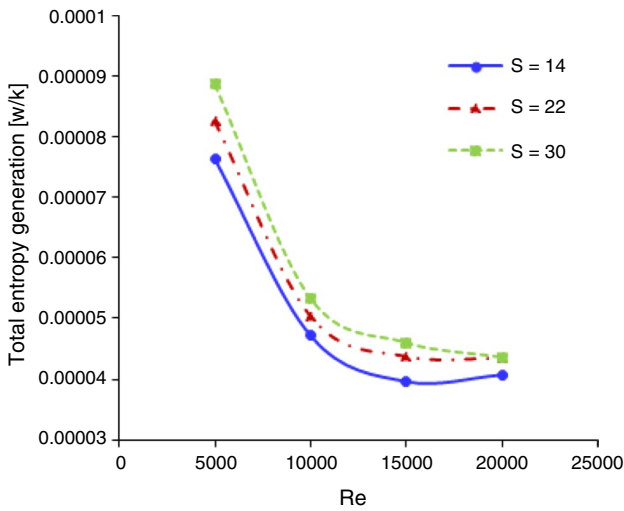


Fig. 14 Changes in total entropy generation versus Reynolds number in different S for $q'' = 3000 \text{ W m}^{-2}$ and $N = 3$

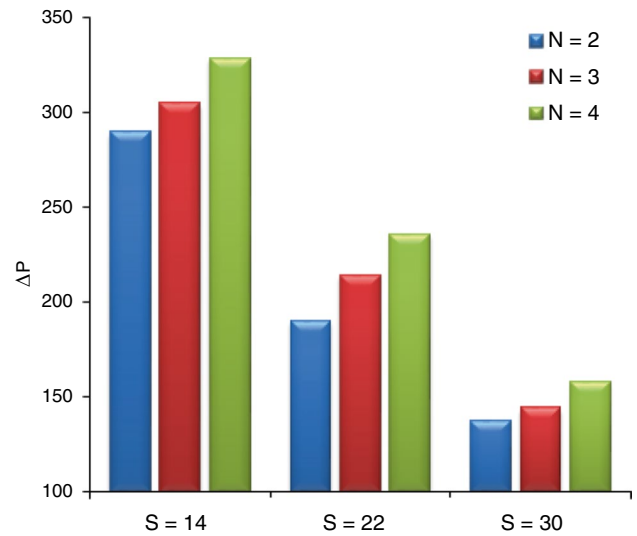


Fig. 16 Variation of pressure drop in pitches at different N at $Re = 1000$ and $q'' = 3000 \text{ W m}^{-2}$

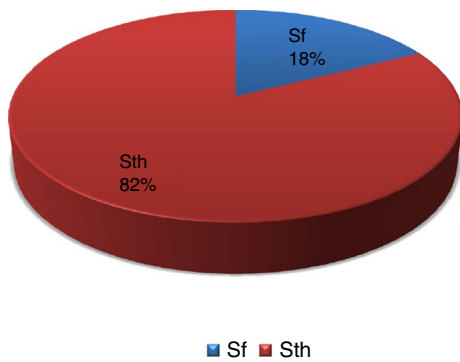


Fig. 15 Circular chart to investigate the contribution of heat and friction entropy on the total entropy generation

According to Eq. (15), increasing the Reynolds number reduces the wall temperature and temperature gradient; and improves the thermal performance. Figure 13b shows that the slope of the graphs decreases with increasing Reynolds number. In fact, the higher the Reynolds number, it has the less effect on entropy generation, indicating that greater Reynolds numbers outcomes less entropy in the same pitch compared to smaller Reynolds numbers.

Figure 14 shows the total entropy changes versus Reynolds number at $N = 3$ and different pitches. It is clear that as the Reynolds number increases, the total entropy also decreases. As mentioned, the total entropy generation consists of two terms: thermal entropy and frictional entropy. It is obvious that with increasing Reynolds number, the total entropy generation decreases, which is due to the total entropy formula mentioned in Eq. (14).

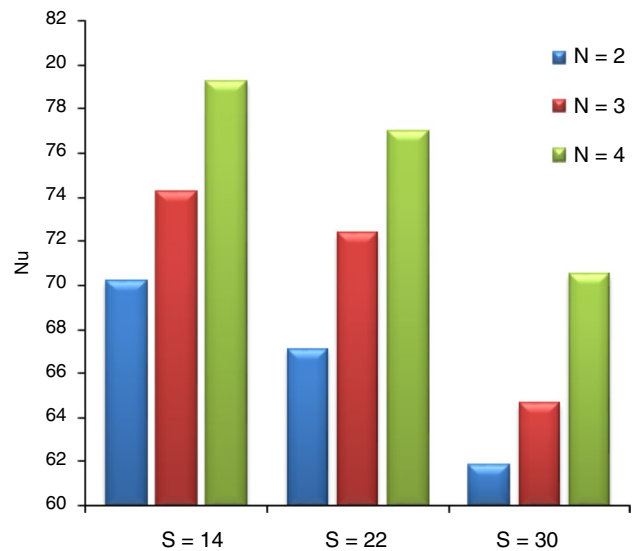
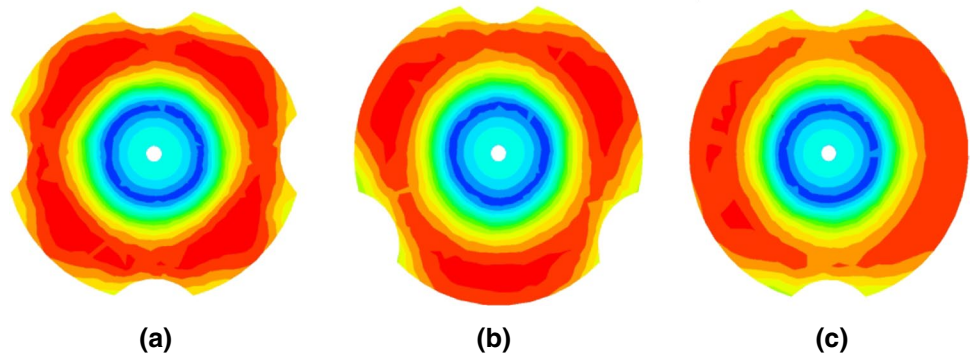


Fig. 17 Nusselt number changes versus number of pitches for different N at $Re = 5000$ and $q'' = 5000 \text{ W m}^{-2}$

The trend of changing the total entropy goes back to the share of each of the heat and friction entropies in the generation of total entropy. Figure 15 is a circular chart, which shows the contribution of each entropy to the total entropy generation, and shows that the role of thermal entropy generation is greater. As explained so far, the effect of thermal entropy is greater. Therefore, the total entropy change is a function of the thermal entropy change, so as the Reynolds number increases, the total entropy decreases.

Fig. 18 Velocity contour in $Re = 15,000$, $S = 14$ mm and in different N on the tube; **a** $N = 4$, **b** $N = 3$, **c** $N = 2$



Investigation of the number of dimples (N) in the cross section

Figure 16 shows the pressure drop changes in the number of different dimples. As can be seen, with increasing number of dimples in the cross section, the pressure drop has also increased. Due to the friction of the fluid with the walls, a pressure drop occurs. In fact, increasing the number of dimples increases the friction and consequently increases the pressure drop.

As shown in Fig. 17, the Nusselt number increases with the number of dimples on the cross section of the tube. In fact, the greater the number of these dimples, the more obstacles are placed against the flow and the longer the flow path of the fluid. The greater the number of dimples, the greater the fluid flow path, resulting in more opportunity for heat transfer and increasing heat transfer. Also, increasing the number of dimples reduces the cross-sectional area, which means a reduction in hydraulic diameter.

From Eq. (11) ($u = (Re \mu) / D\rho$), in a constant Reynolds, the reduction in the hydraulic diameter increases the velocity, which is also shown in Fig. 18. Increasing the velocity reduces the thickness of the thermal and hydraulic boundary layer and also increases the convection heat transfer coefficient which is directly related to the Nusselt number, thus increasing the Nusselt number and increasing the heat transfer.

Figure 19 shows the total entropy changes versus Reynolds numbers at $q'' = 3000 \text{ W m}^{-2}$ and $S = 30$ mm. In a constant Reynolds number, the total entropy decreases with increasing number of dimples, so that the highest total entropy is related to $N = 2$. In fact, thermal entropy determines the overall entropy trend, and as the thermal entropy trend was examined, with increasing number of dimples, the temperature gradient decreased and, consequently, reduced thermal entropy.

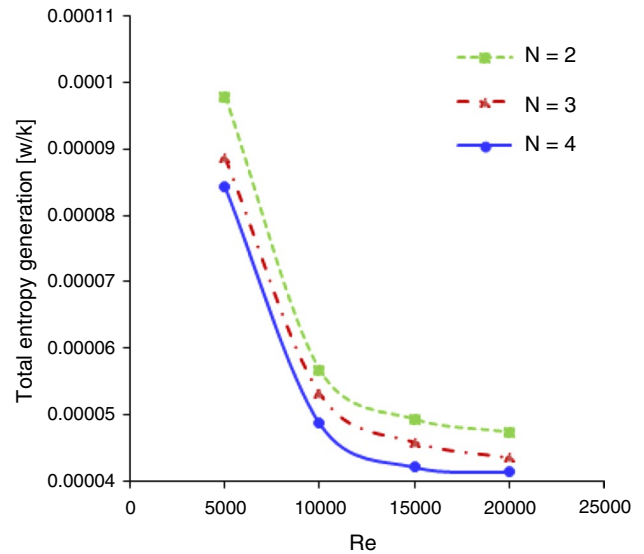


Fig. 19 Total entropy generation changes versus Reynolds number at $q'' = 3000 \text{ W m}^{-2}$ and $S = 30$ mm and different N

Investigation of the effect of applied heat flux

One way to increase entropy production is to increase heat. As the heat flux increases, the temperature of the walls actually increases and the temperature gradient increases. Figure 20 shows the entropy changes generation versus Reynolds number at different heat fluxes at $S = 14$ mm and $N = 2$. It can be seen that with increasing Reynolds number, the total entropy decreases and in a constant Reynolds number, the higher the heat flux causes the higher the entropy. In the previous sections, it was explained that thermal entropy has a greater effect on friction entropy than total entropy generation.

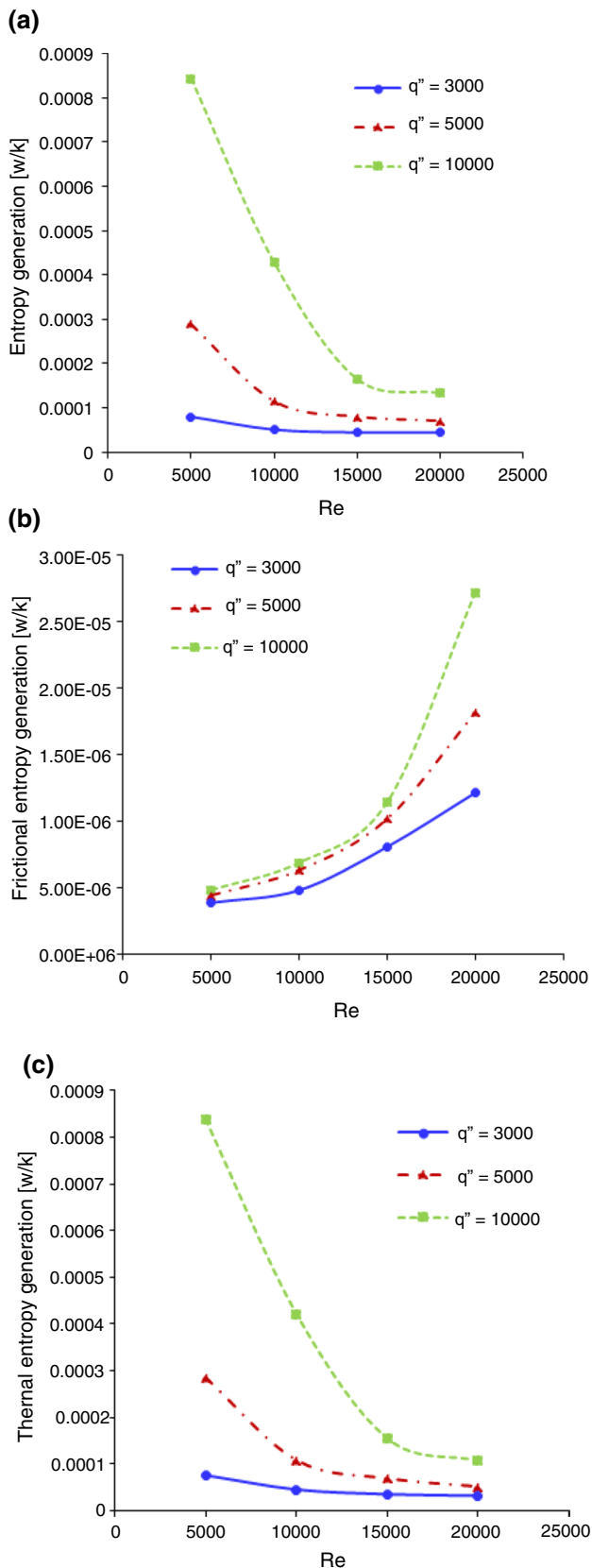


Fig. 20 Variation in entropy: **a** total entropy, **b** frictional entropy, and **c** thermal entropy based on Reynolds number in different heat fluxes, $S = 14$ mm and $N = 2$

Conclusions

This research focused on comprehensive numerical study of heat transfer in a dimple tube equipped with turbulators with regard to consider the first and second laws of thermodynamic. The important point in this research is the numerical investigation of the heat transfer rate and entropy generation by examining the effect of the heat flux, Reynolds number, the pitch (S) and number of dimples (N). The results of this study include the following results:

- As the Reynolds number increases, the frictional entropy increases, the thermal entropy decreases, and since the share of thermal entropy in the total entropy generation is greater, the total entropy decreases.
- Increasing the pitch (S) or decreasing the number of inserted cones (N) reduces the Nusselt number and heat transfer.
- Increasing the pitch (S) reduces the pressure drop and reduces the friction coefficient.
- As the number of dimples or the number of indentations on the tube increases, the Nusselt number increases and causes a decrease in the pressure drop and an increase in the friction coefficient.
- As the number of dimples increases, the frictional entropy increases and the thermal entropy decreases, thereby increasing the overall entropy.
- In low Reynolds numbers, the share of thermal entropy generation is much higher than the friction entropy generation. In fact, as the Reynolds number increases, the share of friction entropy generation in total entropy generation increases.
- The maximum Nusselt number and friction coefficient are at $Re = 20,000$ and the $S = 14$ mm and the $N = 4$, and the heat flux has not significant effect on heat transfer and pressure drop.
- The maximum thermal entropy and total entropy are at $Re = 5000$ and $S = 14$ mm and the $N = 2$, and the maximum frictional entropy is at $Re = 5000$, and $S = 14$ mm and $N = 4$ at $q'' = 10,000$ $W m^{-2}$.

The results of this modeling can be used to obtain the optimal condition to reach the maximum heat transfer rate. For future work, we aim to optimize in order to find the optimal value of each variable.

References

1. Sheikholeslami M, Gorji-Bandpy M, Ganji DD. Review of heat transfer enhancement methods: focus on passive methods using swirl flow devices. *Renew Sustain Energy Rev* 2015;49:444–469.

2. Khanmohammadi S, Mazaheri N. Second law analysis and multi-criteria optimization of turbulent heat transfer in a tube with inserted single and double twisted tape. *Intern J Therm Sci.* 2019;145:105998. <https://doi.org/10.1016/j.ijthermalsci.2019.105998>
3. Kia S, Khanmohammadi S, Jahangiri A. Experimental and numerical investigation on heat transfer and pressure drop of SiO₂ and Al₂O₃ oil-based nanofluid characteristics through the different helical tubes under constant heat fluxes. *Intern J Therm Sci.* 2023;185:108082. <https://doi.org/10.1016/j.ijthermalsci.2022.108082>
4. Khanmohammadi S, Mazaheri N, Bahiraei M. Multi-criterion optimization of a biologically-produced nanofluid flow inside tubes fitted with coaxial twisted tape based on first and second law viewpoints. *Powder Technology.* 2022;412:117930. <https://doi.org/10.1016/j.powtec.2022.117930>
5. Khan MZU, et al. Investigation of heat transfer in dimple-protrusion micro-channel heat sinks using copper oxide nano-additives. *Case Stud Therm Eng.* 2021;28: 101374.
6. Manoram RB, Moorthy RS, Raganathan R. Investigation on influence of dimpled surfaces on heat transfer enhancement and friction factor in solar water heater. *J Therm Anal Calorim.* 2021;145(2):541–58.
7. Rashidi S, Hormozi F, Sundén B, Mahian O. Energy saving in thermal energy systems using dimpled surface technology—a review on mechanisms and applications. *Appl Energy.* 2019;250:1491–547.
8. Thianpong C, Eiamsa-ard P, Wongcharee K, Eiamsa-ard S. Compound heat transfer enhancement of a dimpled tube with a twisted tape swirl generator. *Int Commun Heat Mass Transf.* 2009;36(7):698–704.
9. Wang Y, He Y-L, Li R, Lei Y-G. Heat transfer and friction characteristics for turbulent flow of dimpled tubes. *Chem Eng Technol.* 2009;32(6):956–63.
10. Kumar P, Kumar A, Chamoli S, Kumar M. Experimental investigation of heat transfer enhancement and fluid flow characteristics in a protruded surface heat exchanger tube. *Exp Therm Fluid Sci.* 2016;71:42–51.
11. Li M, Khan TS, Al-Hajri E, Ayub ZH. Single phase heat transfer and pressure drop analysis of a dimpled enhanced tube. *Appl Therm Eng.* 2016;101:38–46.
12. Kukulka DJ, Smith R, Li W. Comparison of condensation and evaporation heat transfer on the outside of smooth and enhanced IEHT tubes. *Appl Therm Eng.* 2016;105:913–22.
13. Shafae M, Mashouf H, Sarmadian A, Mohseni SG. Evaporation heat transfer and pressure drop characteristics of R-600a in horizontal smooth and helically dimpled tubes. *Appl Therm Eng.* 2016;107:28–36.
14. Aroonrat K, Wongwises S. Condensation heat transfer and pressure drop characteristics of R-134a flowing through dimpled tubes with different helical and dimpled pitches. *Int J Heat Mass Transf.* 2018;121:620–31.
15. Aroonrat K, Wongwises S. Experimental investigation of condensation heat transfer and pressure drop of R-134a flowing inside dimpled tubes with different dimpled depths. *Int J Heat Mass Transf.* 2019;128:783–93.
16. Chen J, Li W. Local flow boiling heat transfer characteristics in three-dimensional enhanced tubes. *Int J Heat Mass Transf.* 2018;121:1021–32.
17. Chang SW, Chiang KF, Chou TC. Heat transfer and pressure drop in hexagonal ducts with surface dimples. *Exp Therm Fluid Sci.* 2010;34(8):1172–81.
18. Xie S, Liang Z, Zhang L, Wang Y, Ding H, Zhang J. Numerical investigation on heat transfer performance and flow characteristics in enhanced tube with dimples and protrusions. *Int J Heat Mass Transf.* 2018;122:602–13.
19. Pimsarn M, Samruaisin P, Eiamsa-ard P, Koolnapadol N, Promthaisong P, Eiamsa-ard S. Enhanced forced convection heat transfer of a heat exchanger tube utilizing serrated-ring turbulators. *Case Stud Therm Eng.* 2021;28: 101570.
20. Fang Y, Mansir IB, Shawabkeh A, Mohamed A, Emami F. Heat transfer, pressure drop, and economic analysis of a tube with a constant temperature equipped with semi-circular and teardrop-shaped turbulators. *Case Stud Therm Eng.* 2022;33: 101955.
21. Panahi D, Zamzamin K. Heat transfer enhancement of shell-and-coiled tube heat exchanger utilizing helical wire turbulator. *Appl Therm Eng.* 2017;115:607–15.
22. Eiamsa-ard S, Promvong P. Enhancement of heat transfer in a tube with regularly-spaced helical tape swirl generators. *Sol Energy.* 2005;78(4):483–94.
23. Jasiński PB. Numerical study of the thermo-hydraulic characteristics in a circular tube with ball turbulators. Part 1: PIV experiments and a pressure drop. *Int J Heat Mass Transf.* 2014;74:48–59.
24. Jasiński PB. Numerical study of the thermo-hydraulic characteristics in a circular tube with ball turbulators. Part 2: Heat transfer. *Int J Heat Mass Transf.* 2014;74:473–83.
25. Bashtani I, Esfahani JA, Kim KC. Hybrid CFD-ANN approach for evaluation of bio-inspired dolphins dorsal fin turbulators of heat exchanger in turbulent flow. *Appl Therm Eng.* 2023;219: 119422.
26. Mustafa J, Alqaed S, Sharifpur M. Economic and thermo-hydraulic features of multiphase nanofluids in a heat exchanger equipped with novel turbulators: a numerical study. *Eng Anal Bound Elem.* 2022;144:55–66.
27. Pourahmad S, Pesteei SM, Ravaeei H, Khorasani S. Experimental study of heat transfer and pressure drop analysis of the air/water two-phase flow in a double tube heat exchanger equipped with dual twisted tape turbulator: simultaneous usage of active and passive methods. *J Energy Storage.* 2021;44: 103408.
28. Salhi J-E, Zarrouk T, Merrouni AA, Salhi M, Salhi N. Numerical investigations of the impact of a novel turbulator configuration on the performances enhancement of heat exchangers. *J Energy Storage.* 2022;46: 103813.
29. Mohammed AM, Kapan S, Sen M, Celik N. Effect of vibration on heat transfer and pressure drop in a heat exchanger with turbulator. *Case Stud Therm Eng.* 2021;28:101680.
30. Turgut E, Yardımcı U. Comprehensive analysis of the performance of the coaxial heat exchanger with turbulators. *Int J Therm Sci.* 2022;176: 107502.
31. Nakhchi ME, Hatami M, Rahmati M. Effects of CuO nano powder on performance improvement and entropy production of double-pipe heat exchanger with innovative perforated turbulators. *Adv Powder Technol.* 2021;32(8):3063–74.
32. Ribeiro F, de Conde KE, Garcia EC, Nascimento IP. Heat transfer performance enhancement in compact heat exchangers by the use of turbulators in the inner side. *Appl Therm Eng.* 2020;173: 115188.
33. Liou T-M, Chen C-C, Wang C-S, Wang E-S. Thermal-fluidic correlations for turbulent flow in a serpentine heat exchanger with novel wing-shaped turbulators. *Int J Heat Mass Transf.* 2020;160: 120220.
34. Chen J, Müller-Steinhagen H, Duffy GG. Heat transfer enhancement in dimpled tubes. *Appl Therm Eng.* 2001;21(5):535–47.
35. Bhattacharyya S, et al. Thermal performance enhancement in heat exchangers using active and passive techniques: a detailed review. *J Therm Anal Calorim.* 2022;147(17):9229–81.
36. Pesteei S, Mashoofi N, Pourahmad S, Roshana A. Numerical investigation on the effect of a modified corrugated double tube heat exchanger on heat transfer enhancement and exergy losses. *Int J Heat Technol.* 2017;35(2):243–8.
37. Mashoofi N, Pourahmad S, Pesteei SM. Study the effect of axially perforated twisted tapes on the thermal performance enhancement

- factor of a double tube heat exchanger. *Case Stud Therm Eng.* 2017;10:161–8.
38. Said Z, Rahman S, Sharma P, Amine Hachicha A, Issa S. Performance characterization of a solar-powered shell and tube heat exchanger utilizing MWCNTs/water-based nanofluids: an experimental, numerical, and artificial intelligence approach. *Appl Therm Eng.* 2022;212:118633.
 39. Karami E, Rahimi M, Azimi N. Convective heat transfer enhancement in a pitted microchannel by stimulation of magnetic nanoparticles. *Chem Eng Process Process Intensif.* 2018;126.
 40. Xie C, et al. Performance boost of a helical heat absorber by utilization of twisted tape turbulator, an experimental investigation. *Case Stud Therm Eng.* 2022;36: 102240.
 41. Xu P, Zhou T, Xing J, Chen J, Fu Z. Numerical investigation of heat-transfer enhancement in helically coiled spiral grooved tube heat exchanger. *Prog Nucl Energy.* 2022;145: 104132.
 42. Goh LHK, Hung YM, Chen GM, Tso CP. Entropy generation analysis of turbulent convection in a heat exchanger with self-rotating turbulator inserts. *Int J Therm Sci.* 2021;160: 106652.
 43. Sheikholeslami M, Jafaryar M, Shafee A, Li Z. Nanofluid heat transfer and entropy generation through a heat exchanger considering a new turbulator and CuO nanoparticles. *J Therm Anal Calorim.* 2018;134(3):2295–303.

Publisher's Note Springer Nature remains neutral with regard to jurisdictional claims in published maps and institutional affiliations.

Springer Nature or its licensor (e.g. a society or other partner) holds exclusive rights to this article under a publishing agreement with the author(s) or other rightsholder(s); author self-archiving of the accepted manuscript version of this article is solely governed by the terms of such publishing agreement and applicable law.